January 30, 2006

Seismic Evaluation of Hydrocarbon Saturation in Deep-Water Reservoirs

Grant/Cooperative Agreement DE-FC26-02NT15342.

QUARTERLY REPORT

Report Period Start Date: November 1, 2005
Report period End Date: December 31, 2005

Primary Author: Dr. Michael Batzle

Prime Contractor: Colorado school of Mines
Department of Geophysics
1500 Illinois St.
Golden, Colorado 80401

Subcontractors: University of Houston
Texas A&M University

Industrial Collaborators: Paradigm, Veritas

Principal Investigators:

M. Batzle - Colorado School of Mines
D-h Han - University of Houston (formerly: Houston Advanced Research Center)
R. Gibson - Texas A&M University
Huw James - Paradigm Geophysical

Disclaimer

Abstract

During this last quarter of the "Seismic Evaluation of Hydrocarbon Saturation in Deep-Water Reservoirs" project (Grant/Cooperative Agreement DE-FC26-02NT15342), our efforts have become focused on technology transfer. To this end, we completing our theoretical developments, generating recommended processing flows, and perfecting our rock and fluid properties interpretation techniques. Some minor additional data analysis and modeling will complete our case studies.

During this quarter we have:

- Presented findings for the year at the DHI/FLUIDS meeting at UH in Houston.
- Presented and published eight papers to promote technology transfer
- Shown how Rock and fluid properties are systematic and can be predicted
- Shown Correct values must be used to properly calibrate deep-water seismic data
- Quantified and examined the influence of deep water geometries in outcrop
- Compared and evaluated hydrocarbon indicators for fluid sensitivity
- Identified and documented inappropriate processing procedures
- Developed inversion techniques to better distinguish hydrocarbons
- Developed new processing work flows for frequency-dependent anomalies
- Evaluated and applied the effects of attenuation as an indicator

We have demonstrated that with careful calibration, direct hydrocarbon indicators can better distinguish between uneconomic 'Fizz' gas and economic hydrocarbon reservoirs. Some of this progress comes from better characterization of fluid and rock properties. Other aspects include alternative techniques to invert surface seismic data for fluid types and saturations. We have also developed improved work flows for accurately measuring frequency dependent changes in seismic data that are predicted by seismic models, procedures that will help to more reliably identify anomalies associated with hydrocarbons. We have been prolific in publishing expanded abstracts and presenting results, particularly at the SEG. This year, we had eight such papers to promote technology transfer. Also, we have begun incorporating outcrop descriptive models in seismic forward models.

Our goal for the remaining project period combine the various findings about the deepwater data, present these findings in a unified way and present final conclusions/solutions that can be applied to common problems found in deep water exploration. The final report will be show how we have helped to develop and calibrate techniques to better identify and quantify in situ fluids which will lower risk in drilling new prospects and will improve our capability to monitor fluid motion and exchange in producing reservoirs. These methods now should be tested by industry in actual exploration. To promote this transfer, we are arranging our third DHI mini-symposium in April 2006.

Contents

Figures

Tables

Equations

Project Status

Results

We have demonstrated that with careful calibration, direct hydrocarbon indicators can better distinguish between uneconomic 'Fizz' gas and economic hydrocarbon reservoirs. Some of this progress comes from better characterization of fluid and rock properties. Other aspects include alternative techniques to invert surface seismic data for fluid types and saturations. We have also developed improved work flows for accurately measuring frequency dependent changes in seismic data that are predicted by seismic models, procedures that will help to more reliably identify anomalies associated with hydrocarbons.

We have been prolific in publishing expanded abstracts and presenting results, particularly at the SEG. This year, we had eight such papers to promote technology transfer.

Benefits

This research project has focused on improving our ability to identify and quantify in situ fluids. This lowers the risk in drilling new prospects and improves our capability to monitor fluid motion and exchange in producing reservoirs. The prime benefit locally is an incremental improvement in discovery efficiency and cost. On a larger scale, this also improves our ability to find and assess deep-water resources as a national asset.

Background

Drilling in the deep water environment is expensive and risky. Seismic data has improved to where different pore fluid types can be distinguished. However, many 'dry' holes continue to be drilled, often due to 'false' hydrocarbon indicators.

This project was designed to develop and calibrate techniques to better identify fluid contents at depth. These include methods to make more valid estimates of fluid properties, better ways to calculate the fluid response in rocks, and techniques to distinguish interfering effects resulting from thin beds, low resolution, invasion, etc.

Project Summary

Several approaches have been taken to improve our ability to identify in situ fluids:

– Rock and fluid properties are systematic and can be predicted

- Correct values must be used to properly calibrate deep-water seismic data
- Turbidite reservoirs have geometries that can be identified in field data
- These geometric effects have been quantified and their influence examined
- Hydrocarbon indicators have been compared and evaluated for fluid sensitivity
- Inappropriate processing procedures have been identified and documented
- Inversion techniques have been developed to better distinguish hydrocarbons
- New processing work flows for frequency-dependent anomalies were developed
- The effects of attenuation have been evaluated and applied as an indicator
- A final technology transfer symposium is scheduled for April

Current Status

This project is approaching its conclusion, so our current efforts become focused on technology transfer. To this end, we completing our theoretical developments, generating recommended processing flows, and perfecting our rock and fluid properties interpretation techniques. Some minor additional data analysis and modeling will complete our case studies.

We have now produced improvements in the tools used for in situ fluid identification. These methods now should be tested by industry in actual exploration. To promote this transfer, we are arranging our third DHI minisymposium. The response from industry representatives has been enthusiastic, and several people have already volunteered to present and participate this April.

Accomplishments

We are striving to integrate information and procedures from numerous diverse sources. Samples cover the range from cores, to outcrops, to logs to seismic data. As an example, Figure 1 shows how the productive sheet sand facies seen in outcrop appears on both logs and on seismic data. Turbidite geometries can be complex, but systematic. Understanding the internal architecture allows us to build much more realistic reservoir models. The impact of real heterogeneity is that it could alter the AVO response significantly.

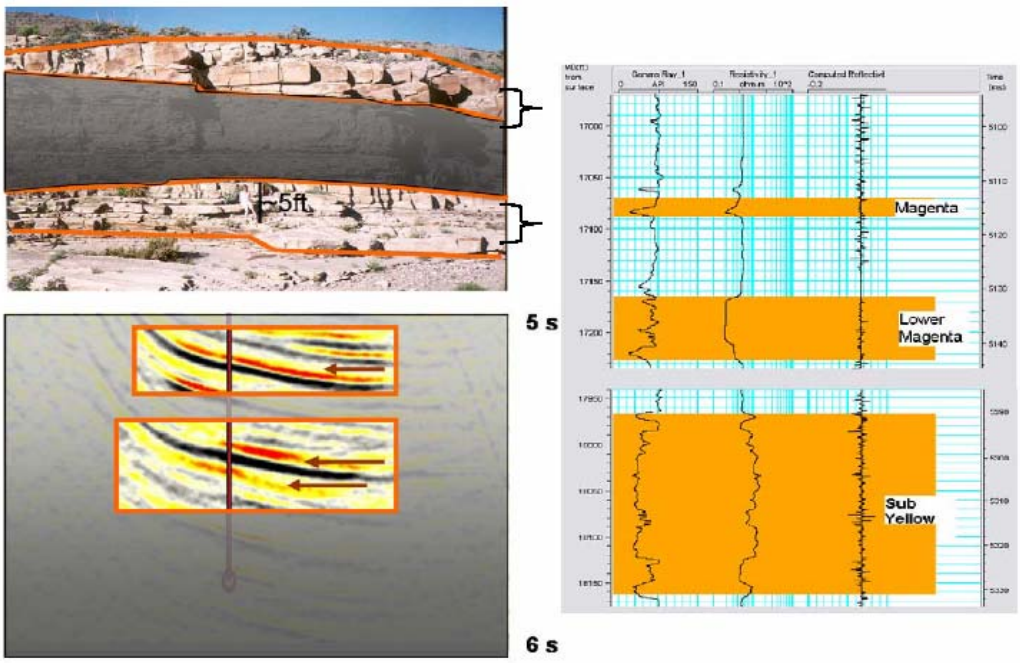

Figure 1. Sheet sand expression in outcrop (a) with wireline (b) and seismic response (c). Note scale of outcrop is almost ¼ that of the seismic. Outlines indicate sheets on seismic and outcrop, highlighted areas indicate sheets in logs.

Other tools have been developed and tested, including examining attenuation as expressed through seismic frequency content. Higher attenuation is expected through partially gas saturated zones. In Figure 2b, seismic amplitude is shown for the King Kong reservoir. By examining a reflector below the reservoir interval (Figure 2b), the low frequency (= high attenuation) ring is seen circling the reservoir.

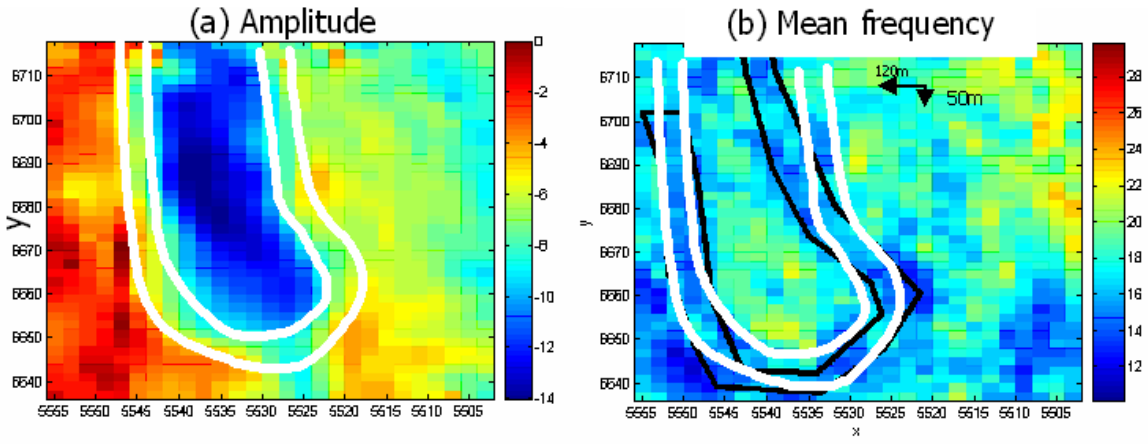

Figure 2. A high attenuation ring is observed around King Kong amplitude anomaly. (a) Near offset amplitude on top sand horizon; (b) Mean frequency below reservoir. The location is shifted down-dip direction: about 120 meters to the leftwards and 50 meters downwards.

We are completing the evaluation of the results of applying frequency-dependent seismic amplitude analysis to several field data sets. The processing methods have been applied to a shallow water site, showing promising results, and are currently being tested on additional deep water data sets with suspected targets of fizz gas and oil reservoirs. This will provide a good opportunity to demonstrate the application of frequency-dependent processing.

Publication

As part of our technology transfer effort, we have submitted and presented numerous abstracts at the Society of Exploration Geophysicists Annual Meeting this November in Houston. These include:

- *Influence of internal reservoir structure on composite reflection coefficients*
- *Robust frequency dependent AVO workflow: Deep water GOM example*
- *Seismic models of turbidite reservoirs*
- *Use of outcrop analogs to predict lithology influence on the seismic signature*
- *Diagnosis of "fizz-gas" and gas reservoirs in deep-water environment*
- *Inversion of Sw and porosity from seismic AVO*
- *Velocities of deep water reservoir sands*
- *Tuning effect on fluid properties estimated from AVO inversion.*

In addition, the specific results of this project are presented in great detail in our Quarterly reports 1 through 12. Annual reports are provided as quarterly reports 4 and 8.

Results and Discussion

Test Sites

There has been continued analysis on data from several target sites. Data and samples have been acquired and most processing is still incomplete (see Table 1 below). Samples were obtained from Kerr-McGee and Marathon Oil Companies. Seismic data has been obtained from Mobil, TGS, and the ERCH consortium. The main tasks to be completed is final interpretations, analysis, and conclusions of results.

Field	Attribute	Status
Nansen	Core samples & logs available	Seismic Obtained, Samples
Viking	Mobil North Sea data with logs	Seismic data and logs acquired
Ursa	Multiple real and false HCI	Seismic analysis begun
Troika	Some data already published	Samples Prep., Veritas 2-D line,
Mars	Published data, salt confined	Veritas 2-D lines, Logs obtained
Boomvang	Near Nansen (Kerr-McGee)	Samples & logs obtained
Mensa	Structurally simple, deep water	Veritas 2-D line, Logs acquired
Teal South	Shelf, only one well, data available	Post-stack data and logs at TAMU

Table 1. Deep-water Gulf of Mexico Fields with seismic hydrocarbon indicators.

Modeling

Composite Reflection Coefficients for Stratified Reservoir Models

We have continued to investigate the properties of seismic waves reservoirs models. The general goal of this work is to understand the limitations of conventional models for investigating the dependence of seismic reflection amplitudes on the angle of incidence of the wave striking the reservoir with amplitude variation with offset (AVO) techniques. Recently, we have examined the dependence of such reflections on the spatial structure of

seismic velocities changes within the reservoir, which is related to the depositional processes that formed the rock layer and, potentially, to its suitability as a hydrocarbon reservoir. We have also made an important advance in that we have completed the development of procedures to design models that more accurately represent the properties of turbidite reservoirs, an important deep-water exploration and production geophysics target.

Influence of internal structure on reflections

Previous reports have described the efficient computation of the composite reflection coefficient using propagator matrix methods. The composite coefficient is the complex-valued amplitude of the total P-wave signal reflected by a plane-layered formation that is somewhat smaller than the incident seismic wavelength. Because the model assumes that the reservoir is composed of horizontal layers, it is possible to solve a simple system of four equations for this amplitude using the propagators.

Previous work applied this method to models that contained a 30 m thick target formation containing 30 internal layers that were 1 m thick. The properties of each layer were independently selected from a Gaussian probability distribution function so that there was no correlation in properties from layer to layer. However, in geological settings like turbidite sequences, velocity will be correlated over distances related to the thickness of sands deposited in a turbidite flow, for example. Such structure can be introduced by applying a von Karman correlation function in the wavenumber domain (Sato and Fehler, 1997),

Equation 1

$$f(k,a,\nu) = \frac{2a(a^2m^2+1)^{-k-1/2}\sqrt{\pi}\nu^2\Gamma(k+1/2)}{\Gamma(k)} \qquad (1)$$

where k is wavenumber and a is correlation length. Results presented here apply n=1/5, where n is a parameter that controls the “roughness” of the model. We also generate models using a Gaussian spatial correlation function, though it is not likely to be provide as realistic a model of typical formations:

Equation 2

$$f(k,a) = \frac{e^{-k^2/(2a^2)}}{\sqrt{2\pi}\sigma} \qquad (2)$$

Examples of models for both of these correlation functions are compared to a model generated with no spatial correlation in Figure 3. Both the exponential and Gaussian models used a=5 m, and all three realizations applied a Gaussian PDF to generate perturbations in the bulk modulus for layers 0.15 m thick. Shear modulus values were correlated with the bulk modulus so that the Vp/Vs ratio remained near 1.8 in all layers.

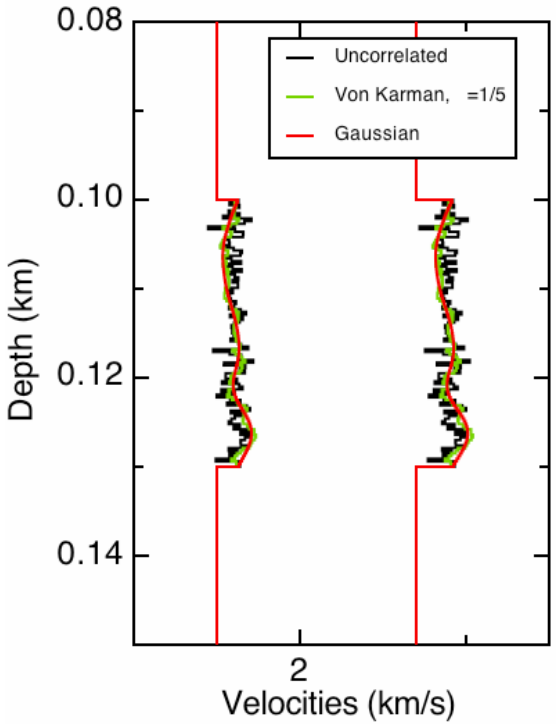

Figure 3. An example realization of each of the model types, one without spatial correlation, and two with the von Karman and Gaussian spatial correlations defined in the text.

For each type of model, 50 realizations were generated using the same random number seed to force models to have the same general velocity fluctuations and to cause the exponential and Gaussian models to have comparable structure (e.g., Figure 3). The magnitude of the P-wave composite reflection coefficient was then computed for an incident plane P-wave with a frequency of 30Hz. Statistical summaries provide a quantitative assessment of composite coefficient results for all model types (Figure 4). The spatially uncorrelated models have the least scatter in amplitudes, because the interference of reflections from the surfaces of each layer tends to cancel out.

However, spatial correlation causes the model to have a few zones of higher or lower velocity, and the reflections from these tend to superpose in more complex ways, leading to more variability. This is especially true for the Gaussian models. We also show amplitudes for simplified, homogeneous reservoir layer models obtained from Backus averaging in this figure. It is interesting to note that the averaging procedure underpredicts the mean response, and it obviously fails to provide any prediction in the variability of the AVO measures.

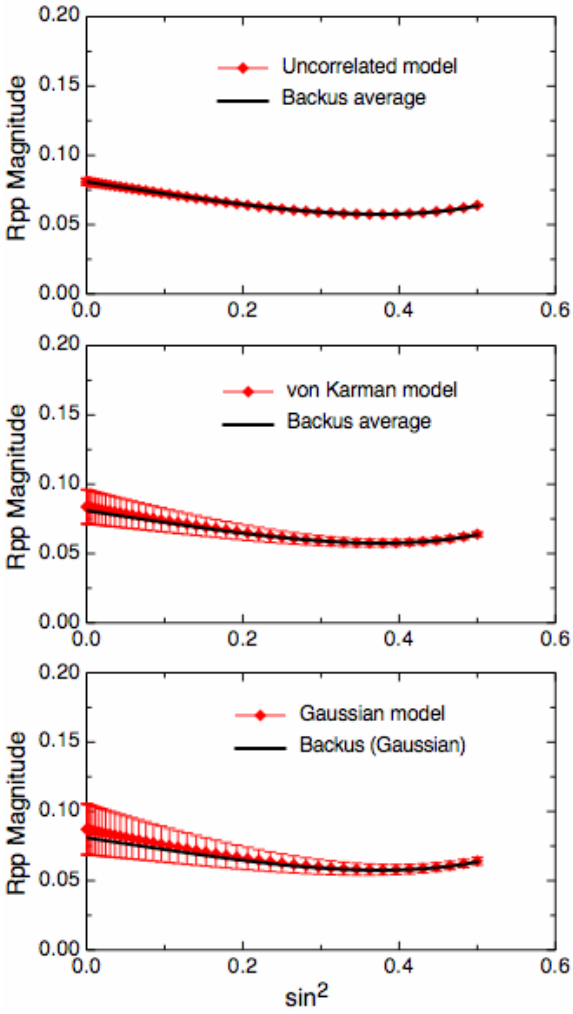

Figure 4. Statistics of the reflection coefficients for composite reflection coefficients generated using the three spatial correlation functions and for the Backus average versions of each model. In each case, 50 realizations were considered. Error bars corresponding to one standard deviation are displayed for the stochastic models, though not for Backus average results which have negligible scatter on the scale of these plots.

Stochastic Turbidite Models

The models discussed in the preceding section are defined using arbitrary distributions of velocity and of spatial correlation. However, specific geologic settings will not likely follow these idealized descriptions. Therefore, we have developed a work flow for generating realistic models of turbidites, including layering and velocity variations. Briefly, the thicknesses of sands and shales are measured using formation microscanner logs, and cumulative distribution functions for the thickness of each lithology are created by tabulating these measurements. Similarly, velocity and density logs provide distributions for these two parameters as well. A specific stochastic turbidite model (STM) is then generated as follows. The model generation begins by specifying a desired total thickness for the turbidite sequence. We then randomly select a bed thickness and a density value from the relevant CDFs, alternating sand and shale until the total thickness is obtained. Examples below use a total thickness value of 30m. If the last layer generated results in a total thickness greater than 30 m, then the thickness of the last bed will be truncated so that the total remains 30 m.

As an example, we used publicly available logs from the Ocean Drilling Program to measure layer thickness, velocity and density from the Amazon Fan. Published studies provide guidelines for correctly identifying layers deposited by turbidites (Pirmez et al., 1997). These distributions are shown in Fig. 5, and they show the characteristic differences in sand and shale properties. To apply the model to Gulf of Mexico studies, the distributions were shifted so that the mean velocities and densities correctly reproduce those found in well logs. We used Vs=Vp/2.25, based on the average of well logs measurements, to estimate shear wave velocity in the models. A sample model is shown in Fig. 6, which compares the STM result to a simpler binary model, a type of model that is often utilized in these studies (e.g., Stovas et al, 2004). Synthetic seismograms generated for this model show that results are frequency dependent, as expected given the structure in the models. Additional results also show that the binary models tend to underpredict the variability in seismic signals, which may be important for practical applications.

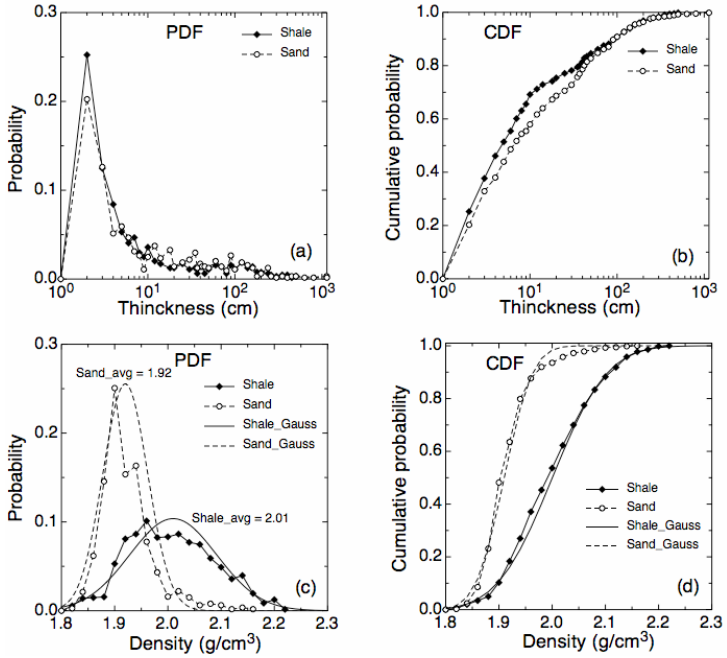

Figure 5. Probability (a) and cumulative density functions of bed thickness (b) for sand and shale beds, and probability (c) and cumulative density functions of density (d) for sand and shale beds.

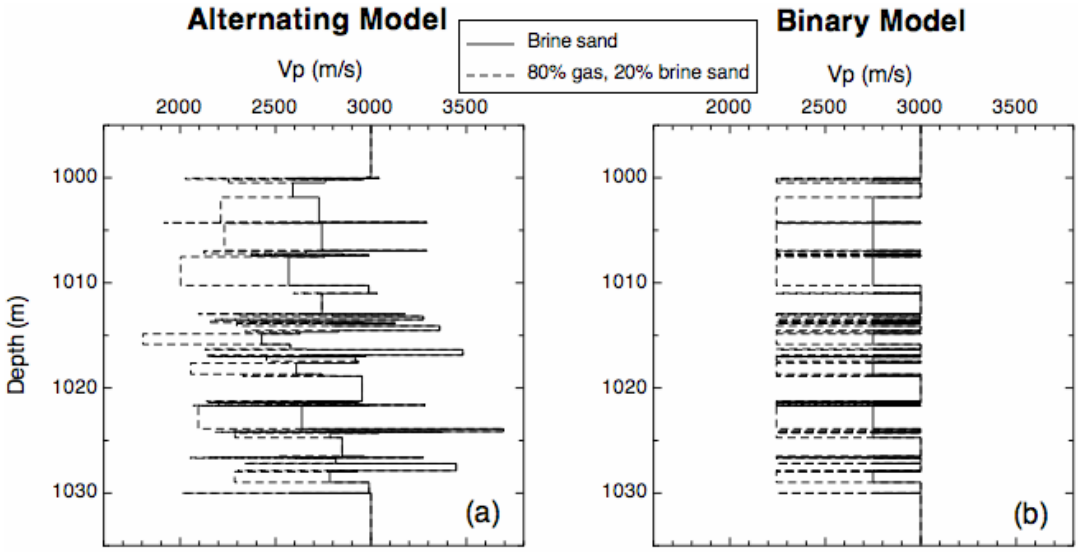

Figure 6. Example of a 30 m thick STM. (a) In the STM, sand and shale beds alternatively appear with a large heterogeneity of layer thicknesses and velocity. (b) In the binary model, the model has the same thickness distribution, but with identical sand and shale properties.

Frequency-Dependent AVO Analyses of Field Data

We have continued our development of methods to improve the detection of frequency-dependent anomalies in AVO measurements, with special emphasis on improved signal-to-noise ratio and avoiding the introduction of processing errors. Our previous study of field data from the Teal South location led to the development of a workflow including a correction for NMO stretch that distorts higher frequencies in the data. Spectral decomposition showed that there was negligible frequency dependence of AVO. A field data set from the Gulf of Mexico presented an additional difficulty because of its relatively low signal-to-noise ratio. This can be improved by "substacking" that data, that is, stacking four adjacent traces in a common reflection point (CRP) gather to suppress noise. We tested this approach on synthetic seismograms to verify its accuracy, and have also tested it on the field data. In addition to greatly improving AVO analysis with minimal distortion of frequency content, it also accelerates the spectral decomposition that is the most time-consuming part of the workflow after migration.

Fig. 7 shows sample field data before and after the substack procedure. Fig 7a shows reflections from two target reservoirs. The NMO stretch is clearly visible at far offset traces, while its correction compacted the wavelet. Also, the alignment of events has been improved significantly resulting in more accurate AVO inversion results. After the spectral decomposition, we barely see any coherent events in high frequency data (Fig 8). After stretch correction, stronger amplitude at far offset from low frequency data has been reduced while very weak amplitude in high frequency data has been recovered. Notice that we only corrected processing artifacts based on the accurate equation that computes the stretch ratio. Though the changes are significant, this correction will not affect any change in frequency content by other factors such as tuning and attenuation. Also changes of amplitude are much smoother due to the substack scheme that increased S/N ratio. Crossplots of two frequency slices over 20 CMP gathers show us significant improvement in our final output (Fig 9). The biased strong low frequency anomaly has been corrected, while background trend only from high frequency data before stretch correction give us accurate attribute information after the stretch correction.

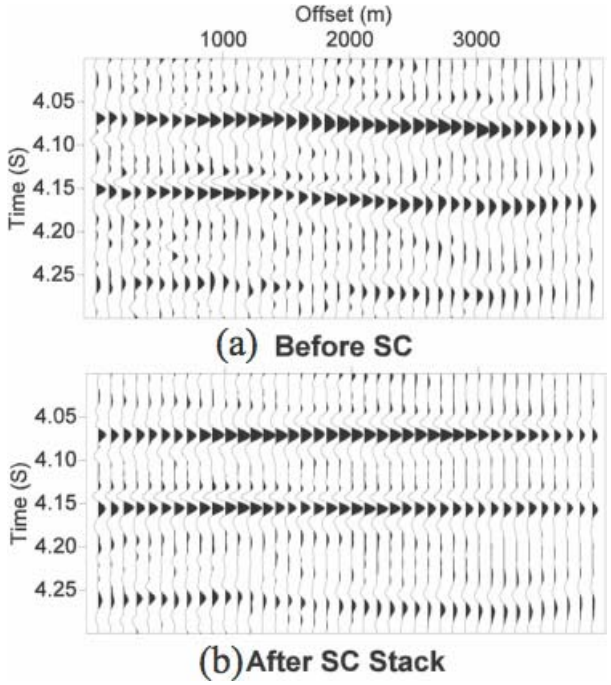

Figure 7. Two GOM deep-water CRP gathers (a) before stretch correction and (b) after stretch correction and substack. Note the increased S/N ratio in addition to improved event alignment. In (a), only every fourth trace is shown for simpler comparison to part (b).

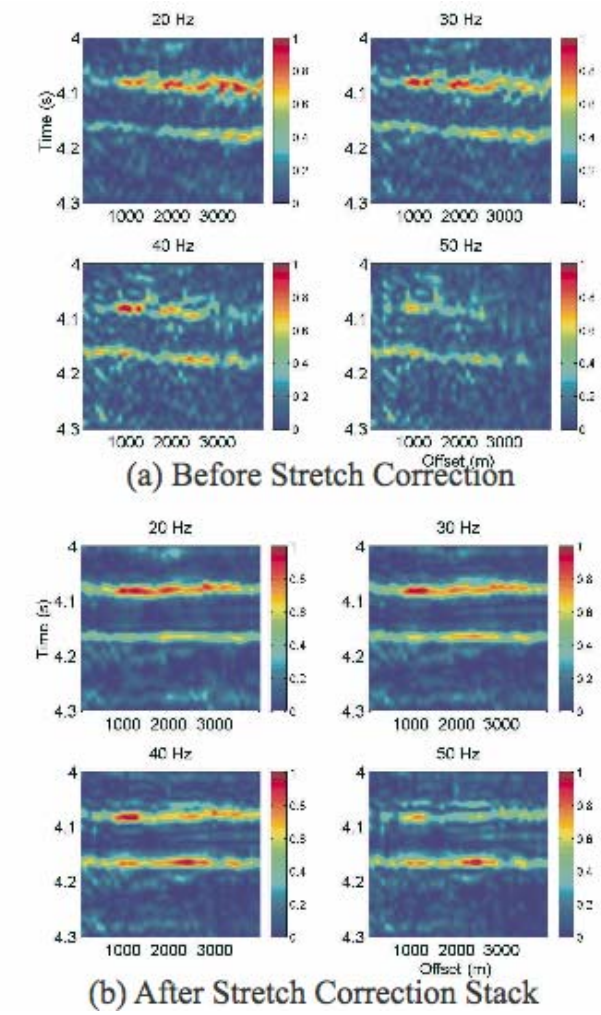

Figure 8. Spectral decomposed prestack gathers (a) before stretch correction and (b) after stretch correction. Each CRP gathers show four frequency slices: 20, 30, 40, 50 Hz. Notice the reduction of the far offset amplitude at 20 Hz and increase of overall amplitude at 50 Hz after stretch correction and stack.

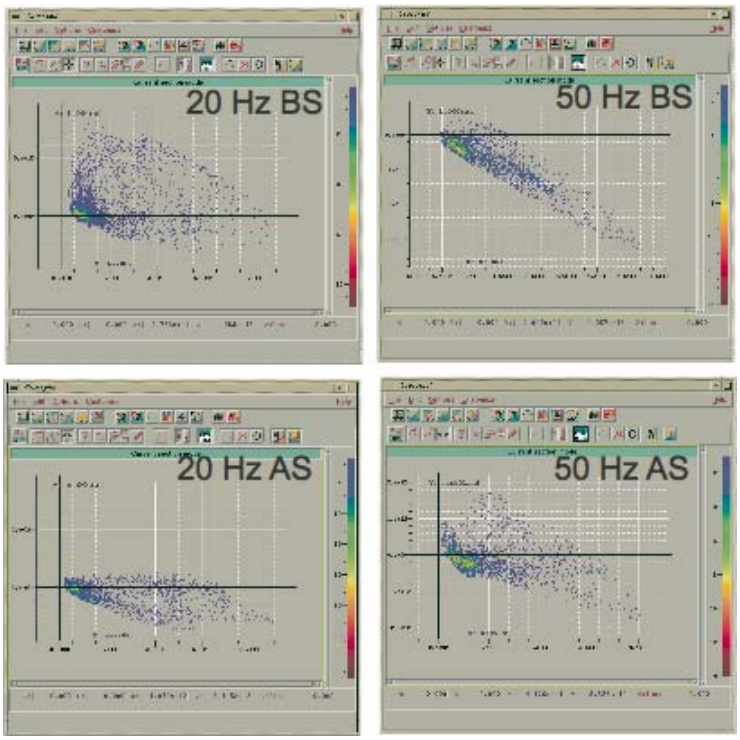

Figure 9. Crossplots of NI and gradient after stretch correction and stack at 20 and 50 Hz. At 20 Hz, false anomaly has been moved to the correction positions, while corrected anomalies show up at 50 Hz. BS: Before Stretch correction, AS: After stretch correction.

Detecting low saturation gas using frequency attenuation

The detection of low saturation gas reservoirs (LSG) using frequency attenuation is tested on field data from the King Kong and Lisa Anne areas in the Gulf of Mexico. The mean frequencies of the seismic wavelets above and below the reservoir are computed and their differences are used to evaluate the frequency attenuation. Well-based synthetic data show the mean frequency has 2 Hz additional frequency attenuation when low saturation gas sand (Q=6) replaces a fully gas saturated sand (Q=30). Measured attenuations from field data around the two wells are consistent with the modeled results: the measured mean frequency decreases about 6 Hz at Lisa Anne and about 4 Hz at King Kong - an additional 2 Hz frequency is attenuated at the Lisa Anne. This example provides a field data evidence that LSG is related to high frequency attenuation, and it is possible to distinguish low saturation gas from commercial gas using the proposed frequency attenuation measurement. A high attenuation (at the level of Lisa Anne) ring around the King Kong field is observed and it may relate to the existence of the transitional, low saturation gas zone around the gas reservoir. The existence of such high attenuation ring may be used an independent (to seismic amplitude) indicator for predicting gas field. Introduction The

low saturation gas sands have similar seismic amplitudes as commercial gas reservoirs, so it is difficult to distinguish the two using seismic amplitudes. Because of this problem in the Gulf of Mexico, the LSG has been considered as the number one risk factor in seismic exploration (O'Brien, 2004). Although it is difficult in detecting LSG using seismic amplitude, it is speculated that LSG may be predicted using frequency attenuation. Based on the lab measurement, the low saturation gas in sandstone can cause strong frequency attenuation (Kumar, et al., 2003) that may be used as an indicator of low saturation gas. Unfortunately, this possibility has not been successfully tested on field seismic data. Part of the reason is that frequency attenuation is difficult to estimate and in most of the cases tuning has a much stronger effect to frequency changes than attenuation (Cobos and Han, 2004). In this report, a new method is tested to measure the frequency attenuation by computing the changes in mean frequencies of the seismic wavelets above and below a reservoir to avoid the frequency tuning around the reservoir reflections. The method is tested on field seismic data from King Kong (gas) and Lisa Anne (LSG) and the measured attenuation matches modeling results. In the first part of the report, the sensitivity of frequency attenuation to quality factor Q is modeled based on the well logs from the two fields. The attenuations from seismic data are computed and analyzed in the second part of the report.

Low saturation gas sands

Figure 10 Shows the King Kong (red) and Lisa Anne (blue) well logs. The Lisa Anne logs are shifted down 57 meters in depth in order to put the first sand tops at the same depth. Three low saturation sands, L1, L2 and L3 are marked in blue at the Lisa Anne well, and three gas sands, K1, K2 and K3 are marked in red at the King Kong well. Obviously, the velocities are very similar between the LSG and gas sands. Because of the similarities between LSG and gas sand properties the seismic responses from the two types of reservoirs are similar and therefore detection of LSG sands from gas sands is difficult by using seismic amplitude alone. More detailed descriptions about the reservoirs can be found in O'Brien (2004). Can frequency attenuation be used to for the detection? It is obviously depends on how low is the quality factor of LSG sand. Based on the previous lab measurement the LSG sands at seismic frequency (Kumar et al, 2003), Q=6 is assigned to LSG sand. Synthetics: sensitivity of frequency attenuation Four models are built based on well data from King Kong (KK) and Lisa Anne (LA) to simulate the gas and LSG scenarios. The model parameters are shown in Figure 11 where two sand layers are inserted in the middle of four shale layers. The parameters of the two sands are shown in Table 2. The rock properties are taken from the well data. The Q values are assigned to sands with different fluids. Some model parameters (underlined) are varied to simulate four scenarios: (1) KK

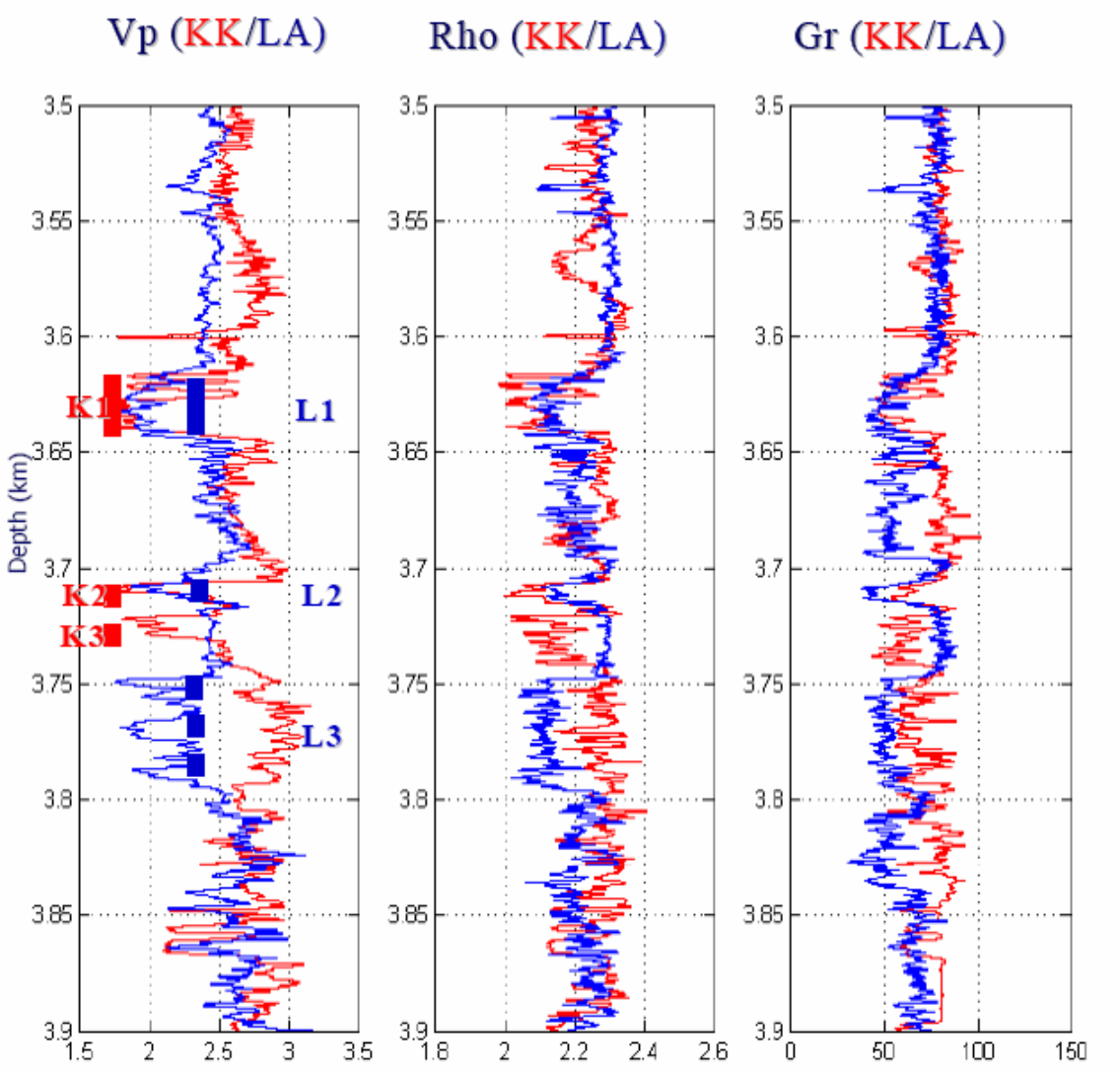

Figure 10. Lisa Anne (blue) and King Kong (red) well logs, from left: Vp, density and gamma ray. Lisa Anne well is shifted down 57 meters in depth to align the first sand top with the King Kong well. The K1, K2 and K3 in red are gas sands at the King Kong well; L1, L2 and L3 in blue are the low saturation gas sands at the Lisa Anne well.

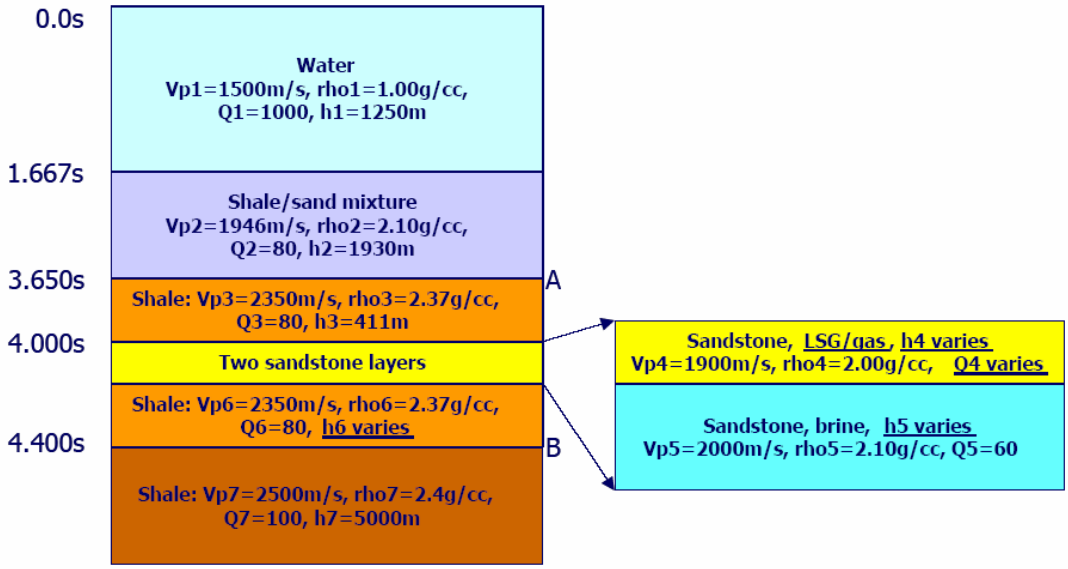

Figure 11. Model and parameters. The parameters underlined varyfor the models listed in Table 2. The thicknesses of the two sands and the shale below, h4, h5 and h6 are adjustedto make sure the two way travel time from interface B is 4.4s. The Q is changed with the fluid in the upper sand.

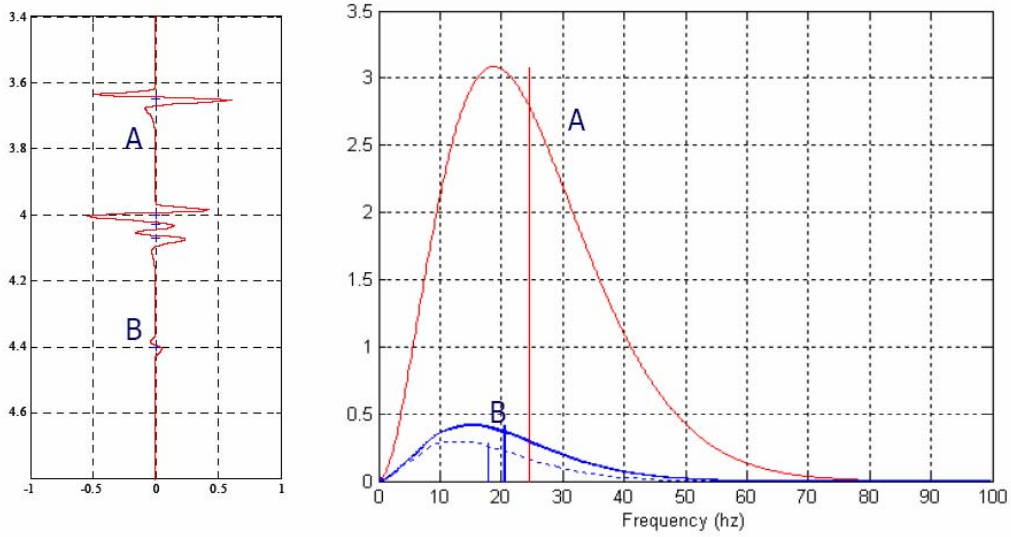

Figure 12. Left: synthetic trace; right: the spectra of the events at A and B for the four models in Table 2. The spectrum of event A is same for all four models. For event B the first three model in solid lines are similar. The fourth model (blue dotted line) with fizz water shows clear difference from the first three models.

	Simulated cases	Sandstone #1			Sandstone #2			Results (hz)		
		fluid	Q	Thickness(m)	Fluid	Q	Thickness(m)	f(A)	f(B)	change
1	KK-1	gas	30	36	brine	60	44	24.62	20.52	4.10
2	KK-2	gas	30	36	brine	60	84	24.62	20.57	4.15
3	LA-g	gas	30	53	brine	60	67	24.62	20.38	4.24
4	LA	fizz	6	53	brine	60	67	24.62	18.32	6.30

Table 2. Model parameters of sandstones and the mean frequencies of seismic wavelets at interfaces A and B in Figure 11 and their differences.

with gas sand, (2) KK with thicker brine sand, (3) LA with gas sand, and (4) LA with low saturation gas sand. The first two models are used to test the sensitivity of the attenuation to the thickness of brine sand. The last three models have the same total sand thickness, so they are used to test the effect of fluids. The differences of mean frequencies at interface A and B are computed as a measurement of frequency attenuation for these scenarios. Figure 12 shows the synthetic data and the spectra of the seismic events at interface A and B that are marked in Figure 11. The spectra of those events are compared in the diagram on the right hand side. The mean frequencies of seismic wavelets at these two points are estimated and listed in Table 2 as f(A) and f(B), along with the measurement of attenuation f(B)-f(A). The results show the attenuation are almost the same for scenarios (1), (2), and (3); implying that the attenuation in frequency is about the same for LA and KK if both reservoirs are gas saturated (with Q=30). From scenarios 1 to 2, the addition of 40 meters of wet sand increases frequency attenuation by 0.05 Hz; from scenarios 1 to 3 the addition of 17 meters of gas sand and 23 meters of wet sand increases attenuation by 0.14 Hz. The results also indicate that the thickness of wet sand (with Q=80) at the tested range affects the frequency attenuation a little. Overall, the sensitivities of frequency attenuation in pore fluids (gas and brine) and sand thickness are relatively small comparing to the existence of LSG. The frequency attenuation increases to 6.3 Hz when the gas is replaced with fizz gas for the last model. This is about a 50% increase in comparison to the first three models. Such change should be able to be observed on seismic data. Unfortunately, direct measurements of the attenuation at the reservoir top and base is difficult because the frequency changes caused by attenuation in many cases are in the same order or even smaller than the change caused by reservoir thickness tuning (Cobos and Han, 2004). The new method described in the next section tries to avoid this problem by measuring frequencies of wavelets above and below the reservoirs rather directly from the reflections of the top and base of the reservoir.

The attenuation measurement

In theory, the frequency attenuation can be computed by measuring the frequency change between the reflections from the top and base of the reservoir. But in reality, such as in Lisa Anne case, which the thickest LSG sand is 27 meters (88 ft) – about 1/3 of the seismic wavelength, such measurement is difficult because it is almost impossible to isolate the top and base events. In this case, the frequency change caused by thickness tuning and by absorption cannot be separated, so the frequency attenuation caused by the low saturation cannot be correctly predicted. In order to avoid the uncertainty of the frequency measurement caused by the tuning, the new method indirectly measures frequency spectra of seismic wavelet at windows above and below the targeted reservoir instead of measuring the frequency change on the top and base of the reservoir. Ideally, if a long seismic window is chosen above or below the reservoir, the power spectrum of the seismic data in the window is the same as the power spectra of the seismic wavelet if the reflection series is random. This can be shown as following. Assume a seismic window $x_t = r_t * w_t$ where r_t and w_t are the reflection series and seismic wavelet, the asterisk denotes convolution. If r_t is a random series with $r_t * r_t = \zeta_t$ at this window, the autocorrelation of the seismic window can be described by $y_{xx} = r_t * w_t * r_t * w_t = w_t * w_t = y_{ww}$. Since the seismic data has the same autocorrelation as the seismic wavelet, they have the same power spectra. With that, the spectrum of seismic wavelet can be estimated at this window. Therefore the mean frequency of the wavelet can be computed. For the field data, a three-step method is used to compute the attenuation. First, windows above and below the reservoir are chosen to compute the spectra before and after the seismic wavelet pass through the reservoir. Second, the mean frequencies are computed for both windows. Finally, the changes of mean frequencies are calculated and used as the measurement for frequency attenuation. The field measurements are interpreted with help of visco-acoustic synthetics shown in the earlier sections. Clearly, choosing a window is an important step of the method in order to have a good estimate of the spectrum of the seismic wavelet. The window length should be long enough to accommodate a reflection series with random features, but it should not be too long and too far from the target so other unwanted factors such as structural variation may affect the spectra of the seismic wavelet.

Field data example

Figure 13 shows two patches from a 3D seismic survey. The two patches cover the King Kong and Lisa Anne reservoirs in Green Canyon in the Gulf of Mexico. The two reservoirs are with gas and LSG respectively (O'Brien, 2004) and thus make the two patches good candidates to test the possibility of detecting fizz gas using the proposed frequency attenuation method. Figure 14 shows the amplitudes on the horizon picked along the top of the sand for the two patches. Two windows (500 ms each) centered at 350 ms above-and 400 ms below this horizon are chosen for spectral analyses. The centers of the two windows are 750 ms apart, same as the time difference in the modeling study. Figure 15 shows the mean frequencies for the windows above (left)

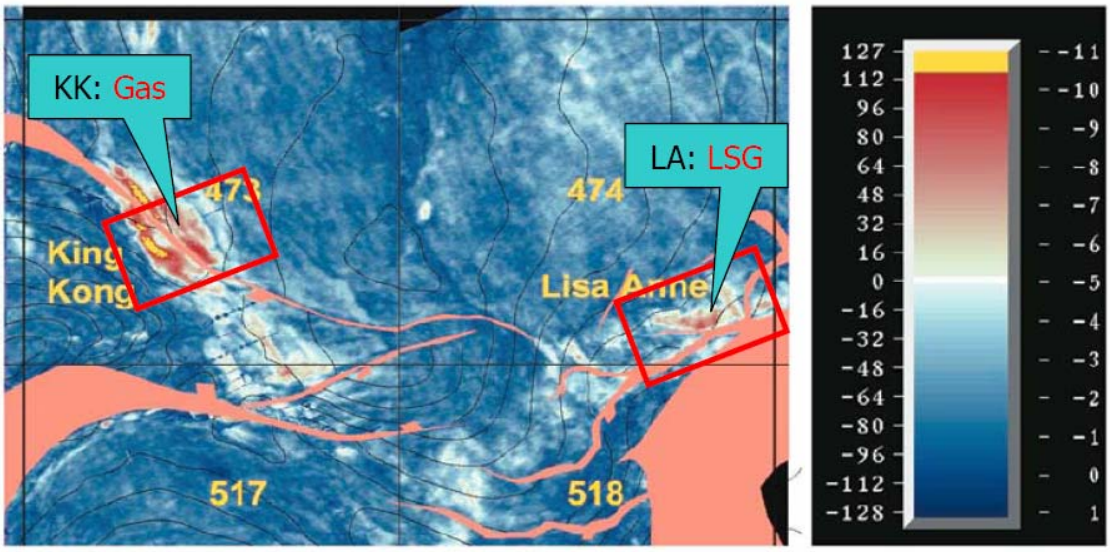

Figure 13. Location of seismic patches around the two wells. The size of the patch is 2080m x 1000m. The two wells are at the centers of the two patches. Based on O'Brien (2004).

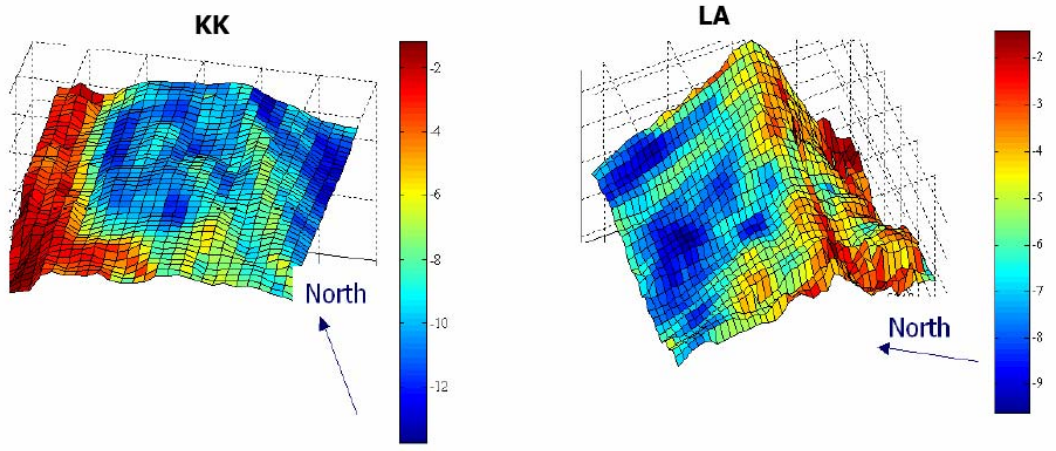

Figure 14. The amplitudes (in color) on the time depths of the top sands for the two patches. Left, King Kong; Right, Lisa Anne.

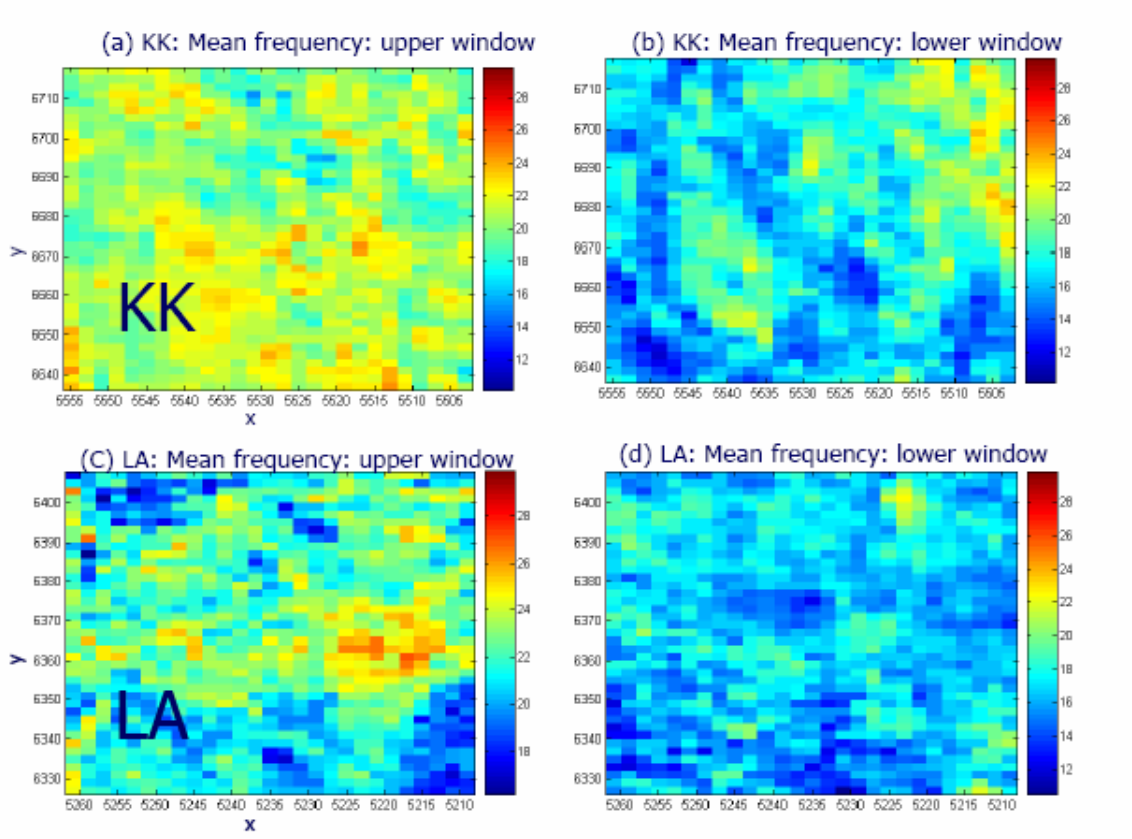

Figure 15. Mean frequencies measured at the windows above and below reservoirs for the two patches.

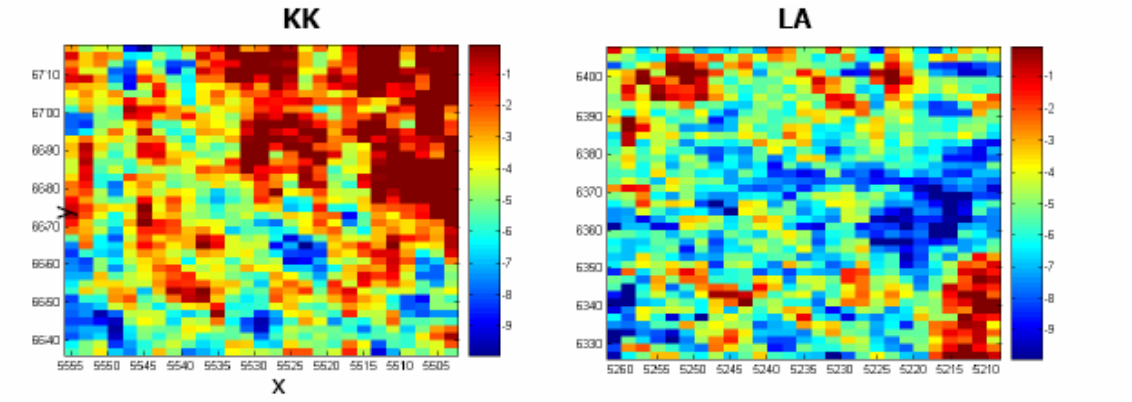

Figure 16. Differences between mean frequencies above and below reservoirs as measures of frequency attenuation. Left for King Kong and right for Lisa Anne.

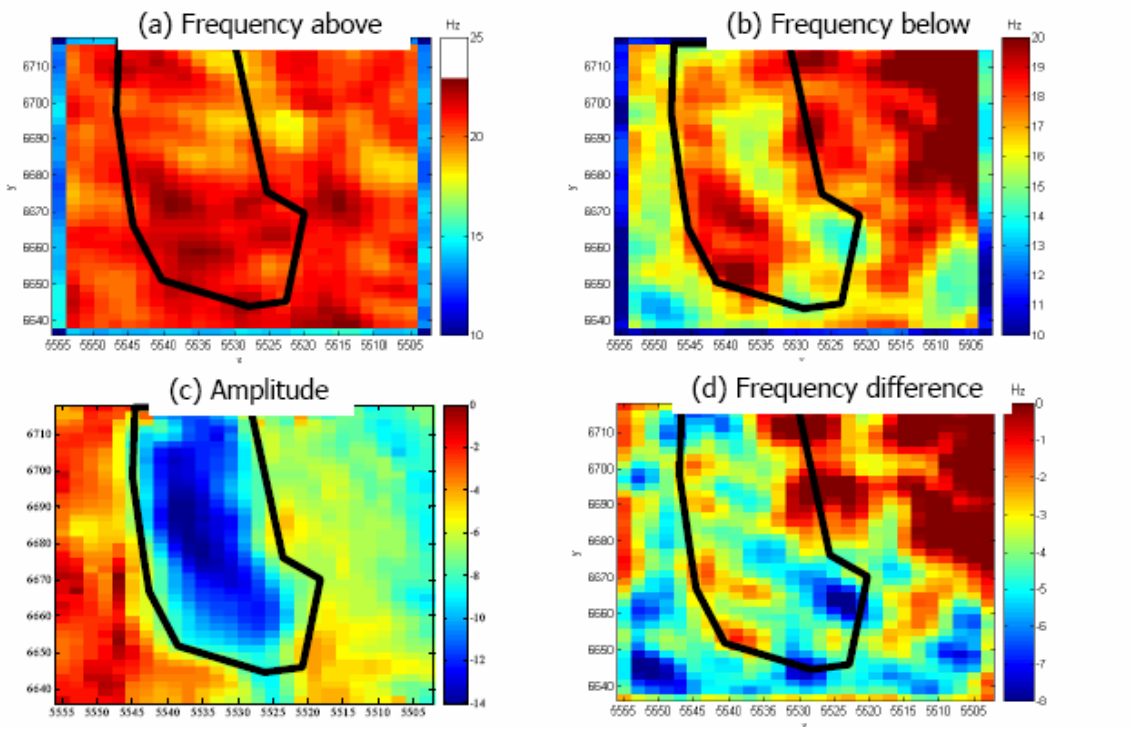

Figure 17. Amplitude, Frequency attenuation analysis at King Kong field. (a) Mean frequency of seismic wavelet at window centered 350 ms above reservoir horizon; (b) Mean frequency 400 ms below reservoir horizon; (c) Seismic amplitude at reservoir horizon; (d) Frequency change between (a)and (b). The polygons in the diagrams show the location of the amplitude anomaly.

and below (right) the reservoirs for King Kong (upper row) and Lisa Anne (lower row). The frequency changes of the seismic wavelets, as the measurements of frequency attenuations are shown in Figure 16 for the two patches. Clearly, there is a high attenuation area in the middle of LA which may related to LSG reservoir. The frequency change is computed by subtracting the mean frequency of the upper window from the lower window, CDP by CDP. This is a good estimation of the frequency attenuation only if the seismic wavelet propagates vertically. In reality, some degree of violation to this assumption can be expected because of the effect of structure and the mis-positioning caused by non-perfect migration. In order to relax this assumption, the estimated mean frequencies are smoothed first before the subtraction. Figure 17, from the top-left clockwise, shows the smoothed mean frequency at the upper and lower windows, the frequency change, and the seismic amplitude at the target horizon for the King Kong patch. A polygon is picked around the amplitude anomaly and this location is marked on the rest of the three diagrams. Figure 18 shows the same contents but for the Lisa Anne patch. Figure 19 shows the histograms frequency attenuation for the CDP's inside the polygons. There is a 2 Hz additional attenuation at the Lisa Anne prospect in comparison to the King Kong field. Some observations are made from the results.

- High frequency attenuation is observed at the Lisa Anne field. This is interpreted as the effect of low saturation gas because the amount of attenuation matches the modeling result previous discussed.
- Can the attenuation be caused by a thick pack of sands? Based on modeled scenarios 1 and 3, adding 17 meters gas sand only increases attenuation by 0.14 Hz. This requires over 200 meters of gas sand to make a 2 Hz additional attenuation. This possibility of having 200 meters of gas sand is unlikely (much stronger amplitude would be expected) by combining the amplitude information. In this case, the joint interpretation of frequency attenuation and seismic amplitude improves the reservoir characterization.
- The high attenuation anomaly at Lisa Anne seems related to the amplitude anomaly in location (Figure 18). The attenuation helps to interpret it as a low saturation gas reservoir. The relation between the attenuation and seismic amplitude is complicated at the lower third of the data because of existence of the fault, so this part of the data is not analyzed.
- Smoothing the mean frequency before computing the frequency difference helps to show the high attenuation anomalies.

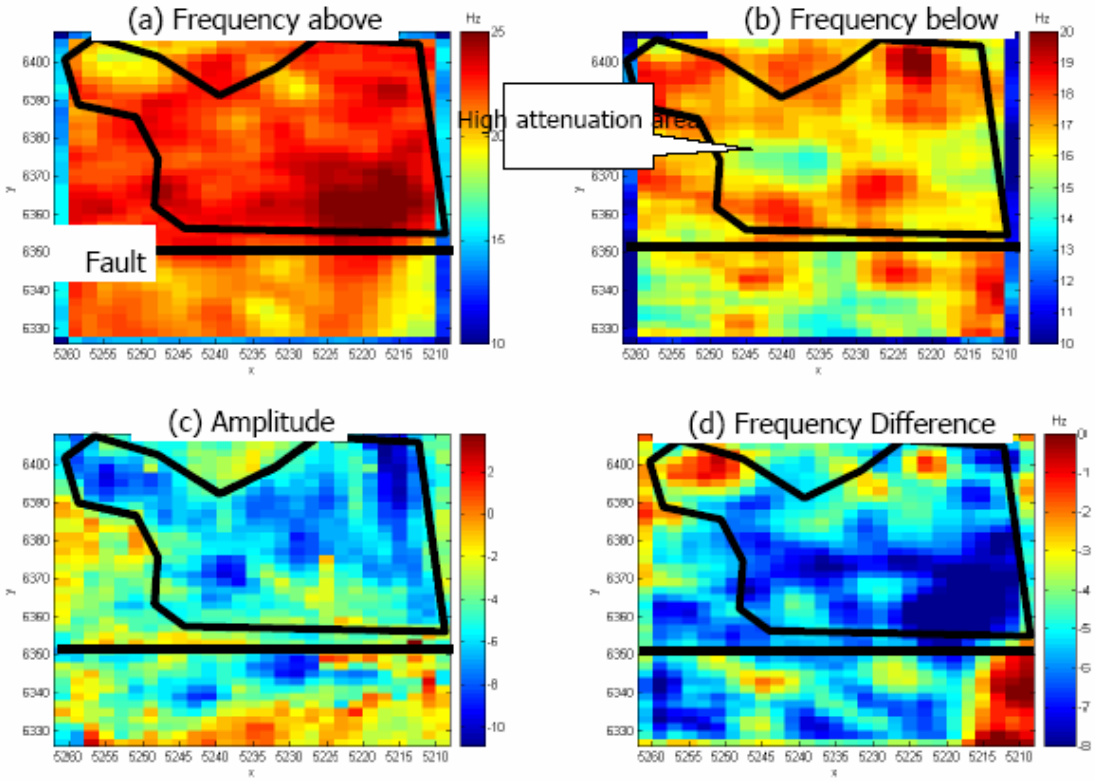

Figure 18. Frequency attenuation analysis at Lisa Anne. See Figure 17 for the description.

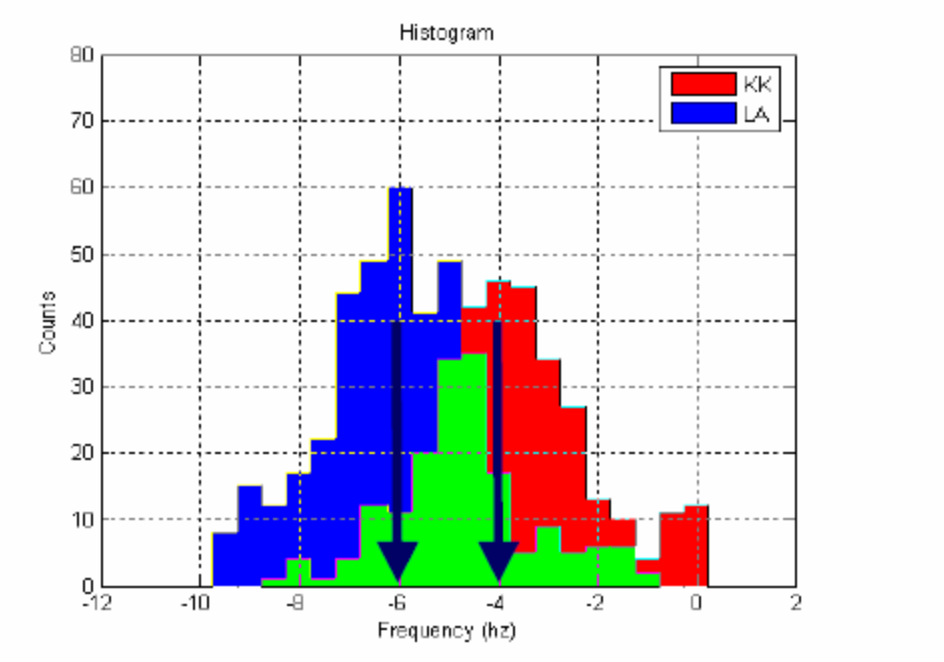

Figure 19. Histograms of the frequency changes for the CDP'sin side the two polygons of the two patches. King Kong and Lisa Anne are colored in red and blue respectively. The overlapped portion is marked in green.

High attenuation ring around gas field – gas to wet transition zone?

A high attenuation ring is observed around the King Kong field. This is marked in black in Figure 20(b). The shape of this ring matches the shape of the amplitude anomaly marked the white lines. It is speculated that this ring is related the high attenuation transition zone between the gas and wet sands. This interpretation is

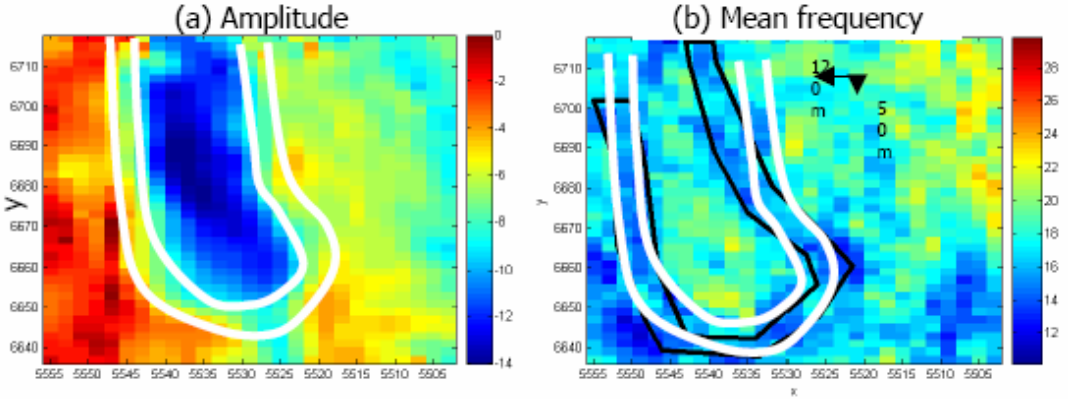

Figure 20. frequencyKKKKGFigure 11. A high attenuation ring is observed around King Kong amplitude anomaly. (a) Near offset amplitude on top sand horizon; (b) Mean frequency below reservoir. The location is shifted down-dip direction: about 120 meters to the leftwards and 50 meters downwards.

supported by two pieces of evidence.

1. There is a great similarity between the shapes of the attenuation ring and the edge of the amplitude anomaly. The position of such ring is shifted down-dip about 120 meters to left and 50 meters downwards. The reason needs to be future investigated. A possibility is that it may be related to the position of the gas/water contact.

2. The mean frequencies (below reservoir) of the King Kong ring and Lisa Anne low saturation gas area are similar.

Figure 21 compares the mean frequencies below two reservoirs for the transition ring, gas field and low saturation gas area. It shows that the ring and LSG have similar mean frequencies and both are about 2 Hz lower than that of the King Kong gas field. The identification of this ring can have a big impact. It may be used as an indicator to detect gas reservoir. This indicator is independent from seismic amplitudes. It does not rely on relative comparison as does for low saturation gas field (as Lisa Anne). The identification of such ring is of important in increasing the confidence of interpreting a reservoir containing commercial gas.

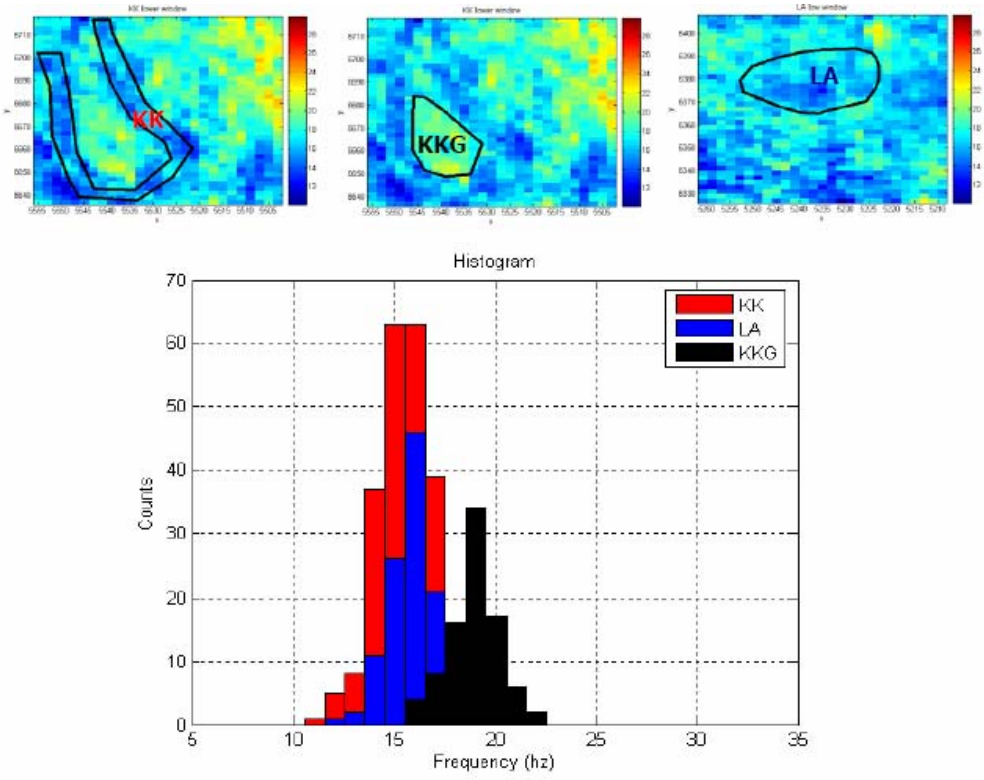

Figure 21. Histograms of mean frequencies of three zones below King Kong and Lisa Anne reservoirs. The three zones marked on the top row on the mean frequency maps are: King Kong high attenuation ring (KK); King Kong gas zone (KKG) and a high attenuation zone at Lisa Anne (LA). The histograms of these three zones are shown on

the lower diagram and the three zones are marked in red, blue and black respectively. The mean frequencies of KKG and LA are similar; but both are lower than KKG.

Discussion

- There is a very small or no attenuation at the upper right corner of the King Kong patch based on Figure 17(d). Either the quality factor in this area is very high or there is some issue with data processing.
- There are some data processing steps that may affect the frequencies of seismic wavelet. Most importantly, the time-variant filtering should never be applied during the processing.
- How faults affect frequency attenuation should be studied in the future.
- The patches are relatively small, only 2080m x 1000m. It is would be helpful to estimate the attenuation for a large area to verify how strong the attenuation anomaly at Lisa Anne relative to the background.

Application/Conclusions

The most important advances that have been made this quarter are related to the technology transfer effort, we have submitted and presented numerous abstracts at the Society of Exploration Geophysicists Annual Meeting this November in Houston. Also we presented results at the DHI/FLUIDS meeting on November 3-4 at the University of Houston.

We have also made important advances in that we have completed the development of procedures to design models that more accurately represent the properties of turbidite reservoirs, an important deep-water exploration and production geophysics target. We have also identified key processing issues that significantly impact data quality such as inappropriate processing procedures which have been identified and documented. New processing work flows for frequency-dependent anomalies were developed and documented and the the effects of attenuation have been evaluated and applied as an indicator. Another method was developed to measure frequency attenuation of the seismic wavelet when it passes through a reservoir. The method can be applied to the case where there exist a few low saturation gas sand layers with high attenuation. Since the method does not measure the attenuation from the reservoir reflector, it is not the affect the thin layer tuning to frequency spectra. The frequency attenuation information is independent of and complimentary to the seismic amplitude and therefore can be used to improve the conventional amplitude interpretation.

Plans

We now have all the data and our intention is to come to some final conclusions on the project and suggest possible topics to explore related with Seismic Evaluation of

Hydrocarbon Saturation in Deep-Water Reservoirs. We have demonstrated that with careful calibration, direct hydrocarbon indicators can better distinguish between uneconomic 'Fizz' gas and economic hydrocarbon reservoirs. Some of this progress comes from better characterization of fluid and rock properties. Other aspects include alternative techniques to invert surface seismic data for fluid types and saturations. We have also developed improved work flows for accurately measuring frequency dependent changes in seismic data that are predicted by seismic models, procedures that will help to more reliably identify anomalies associated with hydrocarbons. In this quarter we have focused much of our efforts on technology transfer. We have been prolific in publishing expanded abstracts and presenting results, particularly at the SEG. We will continue that effort by presenting the final results in the April 2006 DHI/FLUIDS meeting. This will aid in exposing these methods so that they can begin to be tested by industry in actual exploration. In the final months of the project we will prepare to present the final conclusions to what improvements have been made in identification of fluids in deep water environments.

.

Further information can be obtained from:

Dr. Michael Batzle

Colorado School of Mines

Phone: 303-384-2067 email: mbatzle@mines.edu

References

Aki, K., and Richards, P. G., 2002, Quantitative seismology: Theory and methods: 2nd edition, University Science Books, Sausalito, California.

Cobos, C, and Han, D.-H., 2003, Can we use frequency shift due to attenuation for fizz water discrimination? 74rd Ann. Internat. Mtg.: Soc. of Expl. Geophys..

Kumar, G., Batzle, M. and Hofmann, R., 2003, Effect of fluids on attenuation of elastic waves, 73rd Ann. Internat. Mtg.: Soc. of Expl. Geophys., 1592-1595.

O'Brien, J., 2004, Interpreter's Corner—Seismic amplitudes from low gas saturation sands: The Leading Edge, 23, no. 12, 1236-1243.

Pirmez, C., Hiscott, R. N., and Kronen, J. D. J., 1997, Sandy turbidite successions at the base of channel-levee systems of the Amazon Fan revealed by FMS logs and cores; unraveling the facies architecture of large submarine fans: Proceedings of the Ocean Drilling Program, Scientific Results, 155, 7–33.

Shuey, R. T., 1985, A simplification of the Zoeppritz equations: Geophysics, **50**, 609–614.

Stovas, A., Landro, M., and Avseth, P., 2004, Estimation of net-to-gross and fluid saturation in a fine-layered sand-shale sequence—tested on offshore Brazil data: SEG Technical Program Expanded Abstracts, 23, no. 1, 228–231.